Characteristics of plasma properties in an ablative pulsed plasma thruster

Tony Schönherr, Frank Nees, Yoshihiro Arakawa, Kimiya Komurasaki, and Georg Herdrich

Citation: Phys. Plasmas **20**, 033503 (2013); doi: 10.1063/1.4794198
View online: http://dx.doi.org/10.1063/1.4794198
View Table of Contents: http://pop.aip.org/resource/1/PHPAEN/v20/i3
Published by the American Institute of Physics.

Characteristics of plasma properties in an ablative pulsed plasma thruster

Tony Schönherr,[1,a)] Frank Nees,[1] Yoshihiro Arakawa,[1] Kimiya Komurasaki,[2] and Georg Herdrich[3]
[1]*Department of Aeronautics and Astronautics, The University of Tokyo, Bunkyo, Tokyo 113-8656, Japan*
[2]*Department of Advanced Energy, The University of Tokyo, Kashiwa, Chiba 277-8561, Japan*
[3]*Institute of Space Systems (IRS), University of Stuttgart, 70569 Stuttgart, Baden-Württemberg, Germany*

(Received 6 December 2012; accepted 11 February 2013; published online 12 March 2013)

Pulsed plasma thrusters are electric space propulsion devices which create a highly transient plasma bulk in a short-time arc discharge that is expelled to create thrust. The transitional character and the dependency on the discharge properties are yet to be elucidated. In this study, optical emission spectroscopy and Mach-Zehnder interferometry are applied to investigate the plasma properties in variation of time, space, and discharge energy. Electron temperature, electron density, and Knudsen numbers are derived for the plasma bulk and discussed. Temperatures were found to be in the order of 1.7 to 3.1 eV, whereas electron densities showed maximum values of more than 10^{17} cm^{-3}. Both values showed strong dependency on the discharge voltage and were typically higher closer to the electrodes. Capacitance and time showed less influence. Knudsen numbers were derived to be in the order of 10^{-3}–10^{-2}, thus, indicating a continuum flow behavior in the main plasma bulk. © *2013 American Institute of Physics*. [http://dx.doi.org/10.1063/1.4794198]

I. INTRODUCTION

Today's rapid growth in number of satellites, scientific probes, and other in-space applications yields the demand for reliable and versatile space propulsion systems. Recent years have seen an increasing number of satellites equipped with electric propulsion instead of the well-established chemical propulsion due to their significant advantage with regard to propellant consumption, and the related savings of wet system mass.[1] Among electric propulsion systems, the pulsed plasma thruster (PPT) can offer a wide range of performance depending on design and energy input, and therefore, might be suited for various applications, especially with regard to small satellites down to cubesats.[2] Several PPT were applied in the past to serve, e.g., as attitude control system or for North-South station keeping on a fair number of satellites.[3,4]

In solid-ablative PPT (SPPT), the energy stored in a capacitance is discharged across the surface of the solid propellant (most often PTFE) in order to disaggregate it into a plasma and accelerate the charged particles by the self-induced magnetic field.[3,5] For initiation of the discharge, an igniter is used to shortcut the open oscillation circuit. A schematic image of the thruster is shown in Figure 1.

The impulse created during the short-time discharge is in the order of a few 10 μNs for microPPT up to 1 Ns for high-energy devices. The energy and especially the combination of capacitance and discharge voltage have significant effect on the discharge behavior,[6] the plasma acceleration,[7] and the efficiency of the thruster alike.[8,9] It is, therefore, to be expected that the properties of the plasma in terms of temperature and density will show a strong dependence on these parameters as well.

Previous research assumed that the ablated and ionized mass will be accumulated in a so-called current sheet that is accelerated down the channel formed by the electrodes. However, this phenomenon was only observed for gas-fed PPT,[10] but similar high-speed camera measurements in solid-ablative PPT showed no distinct current sheet but rather a diffuse plasma bulk.[7,11–13] Further, measurements of the current density in the discharge space showed that the discharge current, and its induced magnetic field, was concentrated close to the propellant surface area during the entire discharge time, and was not or only slightly moving through the channel in contrast to what was previously assumed.[12,14–16] Due to recent capabilities in simulating the ablation process, it was also shown that the ablation rate, and hence, ionization rate of the used PTFE strongly depends on the discharge current and is therefore a strong function of time.[17–20] This would again favor the idea of a distributed plasma bulk rather than a distinct concentrated sheet.

In order to evaluate how the plasma properties, i.e., electron temperature and electron density, are distributed in the discharge channel, two optical methods were applied in this study. First, optical emission spectroscopy was used to derive the values as a function of time, space, discharge voltage, and main capacitance. Previous experiments showed that the method is suitable to be applied to PPT.[21,22] Second, Mach-Zehnder interferometry (MZI) was used to derive the values for comparison and increase in reliability. Although MZI is a well-established method for highly transient plasma phenomena,[23–25] due to the expected low electron quantity of $\mathcal{O}(10^{16}\text{cm}^{-2})$ in the optical path of the light source, it was hardly applied to PPT before.[26] This present work shows the evaluation of the experimental data and their limitations.

The plasma properties are of further interest for the numerical simulation of the plasma phenomena in order to verify their results for, e.g., the coding efforts in Germany[27–29] as well as for additional refinements of the established slug performance model.[9] With the values of temperature and density, further plasma characteristics like Debye length and

a)schoenherr@al.t.u-tokyo.ac.jp.

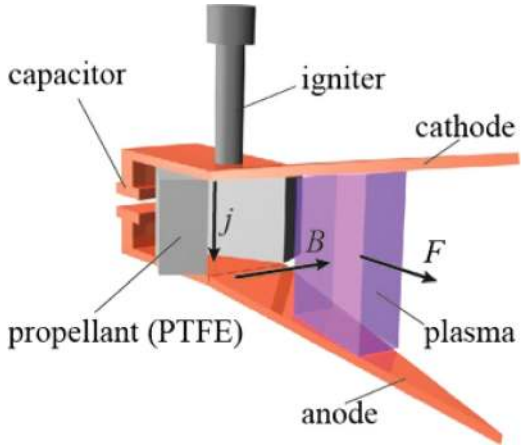

FIG. 1. Operation schematic of a pulsed plasma thruster.

Knudsen number are derived. These can help to understand better the nature of the plasma during the discharge of the PPT.

II. EXPERIMENTAL SETUP

A. Thruster and vacuum environment

For the experiments in this study, an engineering model of the ablative pulsed plasma thruster ADD SIMP-LEX is used which has been explained in detail elsewhere.[8] The thruster consists of a pair of copper electrodes connected to up to four capacitors with each 20 μF. A semiconductor spark plug is used as igniter, and PTFE as propellant in a side-fed configuration. The capacitors are rated to 1300 V which yields a maximum discharge energy of 68 J. At this energy level, the thruster produces an impulse in the order of 1 mNs per pulse.

The vacuum facility used for the study comprises a grounded vacuum chamber of 500 mm in diameter as well as a rotary vane pump and a turbo molecular pump providing a throughput of 2.2×10^{-3} Pa m^3/s at 0.01 Pa. The background pressure during the experiments was typically below 5×10^{-2} Pa.

B. Emission spectroscopy

The spectrometer used for measurement of the plasma emission is a LTB Echelle spectrometer type Aryelle 200 together with an Andor Technology iStar CCD camera. The spectrometer has a wavelength range of 232-828 nm, and a resolving power of around 9000. A traversable lens system is used to alter the focal point as is shown in the schematic Fig. 2. Calibration of wavelength was done using a mercury lamp, intensity standardization by means of a 45 W quartz-halogen tungsten coiled filament lamp. Nine measurement points were considered to evaluate the spatial distribution of the plasma. These points are shown in the inset in Fig. 2. The shutter of the spectrometer was kept opened throughout the experiments, whereas the signal amplification in the CCD camera was controlled directly by a pulse generator. This enabled virtual exposure times of 500 ns resulting from a compromise between temporal resolution and sufficient signal-to-noise ratio. Due to the transient character of the discharge, several spectra were recorded at each point to cover the entire discharge time of $\approx$12 μs. Due to internal hardware delays of spectrometer and photo detector, the minimum delay of the measurement is 1 μs.

C. Mach-Zehnder interferometry

Two-wavelength MZI was carried out by using a 12 mW He-Ne laser (633 nm) and an 8 mW YAG laser (532 nm) as probe lights. The probe light is split before the vacuum chamber allowing for one beam to pass through the plasma, whereas the other beam stays uninfluenced. An interference pattern is created by inflicting an optical retardation at recombination of the beams. The pattern is then recorded with a DRS Hadland Ltd. Ultra-8 high-speed framing camera at typical exposure times of 250 ns by a 520×520 pixel image. In order to increase the sensitivity of the system, the real beam diameter was kept smaller than the plasma bulk, requiring a total of four images to cover the complete plasma. In order to avoid perturbations of the image due to the emission from the plasma, band-pass filters were used before the camera entry. The entire setup is shown in Fig. 3.

III. EXPERIMENTAL RESULTS

A. Emission spectroscopy

Emission spectroscopy was conducted at the 9 measurement points as shown in Fig. 2 for 5 discharge voltages between 500 and 1300 V and for the highest voltage also for

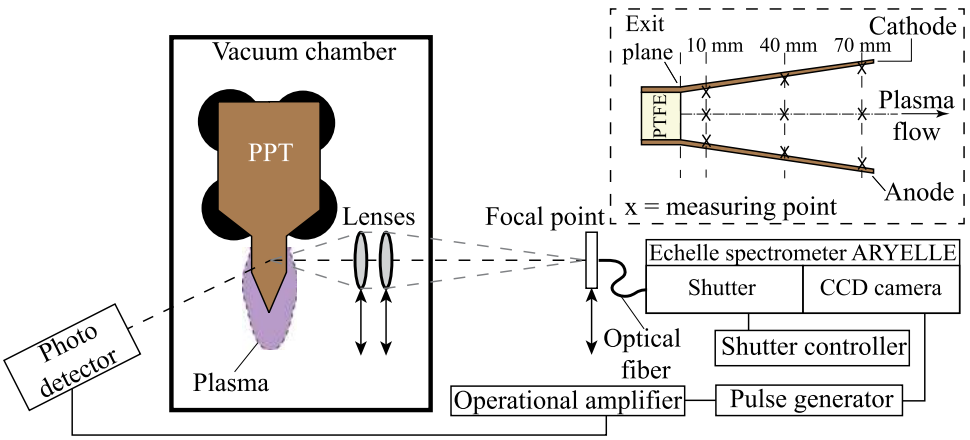

FIG. 2. Setup for measurements using optical emission spectroscopy (inset showing the measurement points).

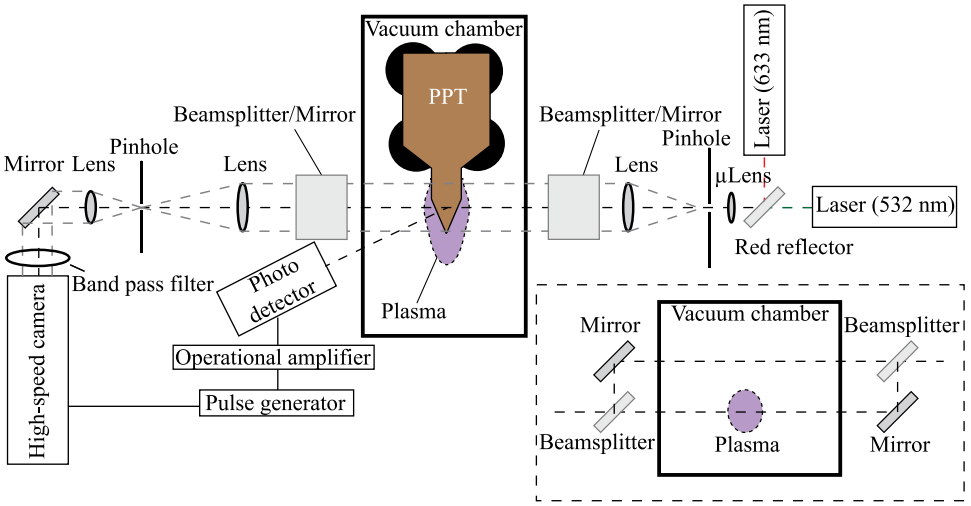

FIG. 3. Setup for measurements using Mach-Zehnder interferometry.

a reduced capacitance of 20 μF. The recordings were deliberately delayed to analyze the plasma through the entire discharge time. Comparison with the discharge voltage signal was used to confirm the timing of the spectrum, and the time stamps stated hereafter refer to the time after discharge ignition. For the complete discharge plasma, i.e., from 0 to 12 μs, a typical recorded spectrum is shown in Fig. 4. The spectral lines of carbon and fluorine lines were easily identified, and compare well with the composition found for other PPT.[12,21,30]

Figure 5 shows the spectra for a position 10 mm downstream of the propellant for the 3 measurement points in the cross section. Besides the difference in spectral intensity that was indicated already by high-speed camera measurements, it is further obvious that the composition of the plasma in the cross section is not uniform and not symmetric. Especially, one can see that the most intense lines at the points close to the electrodes belong to C II, whereas strong emission from C III is seen on the center line. This indicates an energy distribution that is non-uniform across the ablation surface which should also be represented by the electron temperature and electron density, respectively.

Regarding the energy level, 3 representative spectra are shown in Fig. 6. Decrease of discharge energy by either a decrease in bank capacitance or discharge voltage leads to a decrease of intensity as expected, but again shows differences in the composition of the plasma emission. A lower capacitance of 20 μF (Fig. 6(a)) yields a significantly reduced emission from C III, indicating that the multiply-ionized species are not as likely to be created as at the condition of higher capacitance of 80 μF (Fig. 6(b)). A reduction of the discharge voltage, however, more strongly decreases the overall emission intensity, but shows similar composition of the plasma (Fig. 6(c)). It is, therefore, valid to assume that the ablation and ionization processes are influenced by these parameters differently, and that this should again be reflected by the electron temperature and electron density.

To derive the excitation temperature of the individual species, the appropriate spectral emission lines were fitted by a Voigt function, and the integrated results arranged in a Boltzmann plot. An exemplary fitting is shown in Fig. 7(a) and an exemplary Boltzmann plot is shown in Fig. 7(b) for the fitted values of C II. Similar to previous research,[21] it cannot be concluded unambiguously whether or not LTE is present. As similar tendencies with occasionally fewer reliable spectral emission lines to use were derived for other time stamps, other measurement points, and other discharge voltages, as well as for F II, the indications are nevertheless significantly high that LTE can be assumed.

From the slope of the Boltzmann plot, an excitation temperature can be derived, that is equal to the electron temperature under the above-made assumption of LTE. For the nine measurement points and as a function of the elapsed time after ignition, the excitation temperature was derived for the highest energy configuration of the thruster, and is plotted in Fig. 8. Note that the peak in discharge current is around $t = 2.5$–3.0 μs, and that the plasma moves at a velocity of about 40 mm/μs. The results indicate that the temperature is higher closer to the electrodes which would confirm the observations of a higher emission intensity in Fig. 5. As the plasma moves downstream, the temperature changes only slightly, therefore, indicating that not much energy is lost during the acceleration process. As the current density is relatively small in this part of the plasma,[16] it is expected

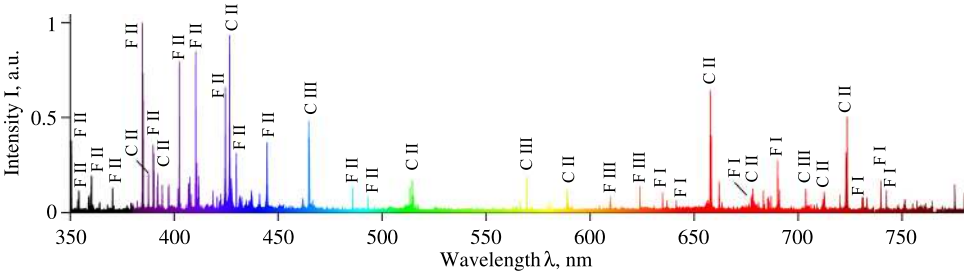

FIG. 4. Long-exposure emission spectrum of PTFE plasma.

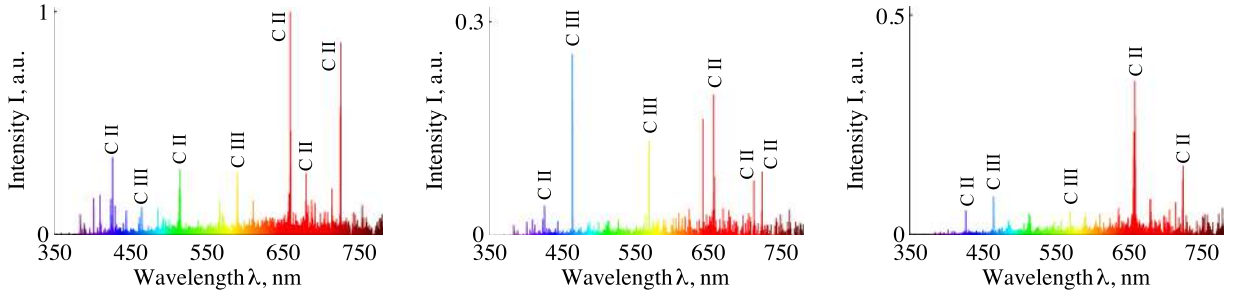

FIG. 5. Emission spectra at 3 measurement points for $x = 10\,\text{mm}$, $U = 1300\,\text{V}$, $C = 80\,\mu\text{F}$, and $t = 2.6 - 3.1\,\mu\text{s}$.

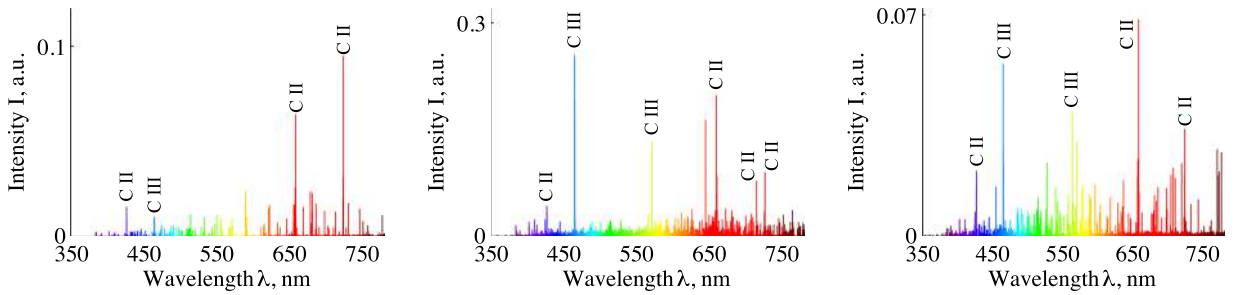

FIG. 6. Emission spectra at $x = 10\,\text{mm}$, centerline, and $t = 2.6 - 3.1\,\mu\text{s}$.

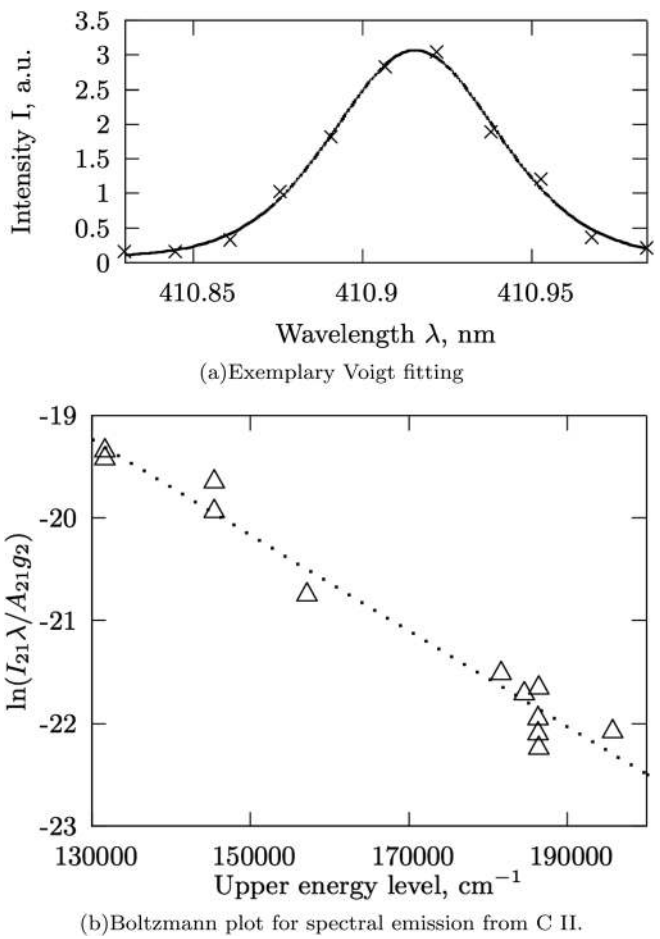

FIG. 7. Exemplary analysis results of the experimental spectral data.

that radiation losses as well as Ohmic heating are negligibly small, which would support the fact of a hardly changing temperature. Temperature close to the cathode decreases, whereas the temperature on the centerline increases. Essentially, at $x = 70\,\text{mm}$, the plasma has an almost uniform temperature of about 2.25 eV across the cross section. This fast temperature exchange process would indicate that the ion density is significantly high enough. The derived values of excitation temperature agree quite well with findings of other research groups having found a temperature of 1.4 eV (at 45 J),[21] or values up to 5 eV by Langmuir probe measurements (at 20 J).[31]

The electron density is derived by using the FWHM of the Stark broadening effect Γ of the spectral emission lines that were fitted by a Voigt profile, and compare it to the theoretical value for iteration of the electron density. Therefore, the Lorentzian contribution to the profile needs to fulfill the following empirical equation (with n_e in m^{-3})[32]

$$\Gamma_L = 2W\left(\frac{n_e}{10^{22}}\right) + 3.5A\left(\frac{n_e}{10^{22}}\right)^{1/4}(1 - 1.2 \cdot n_D^{-1/3})W\left(\frac{n_e}{10^{22}}\right), \tag{1}$$

where the parameter n_D is defined as

$$n_D = 1.72 \cdot 10^{12}\frac{T_e^{3/2}(eV)}{n_e^{1/2}}. \tag{2}$$

The parameters W and A are taken from literature[33] and interpolated for the given temperature. In the calculation process, the assumption was used that the electron temperature equals the excitation temperature. The results are plotted

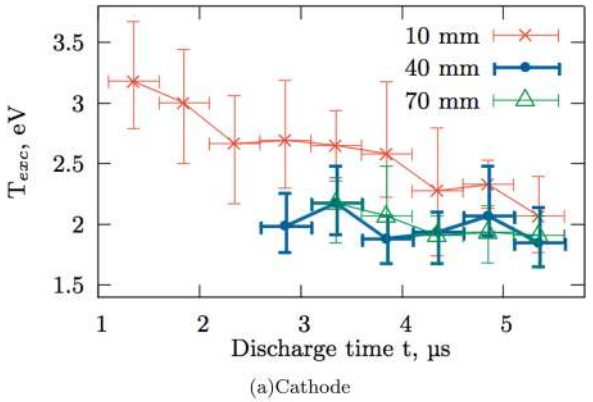

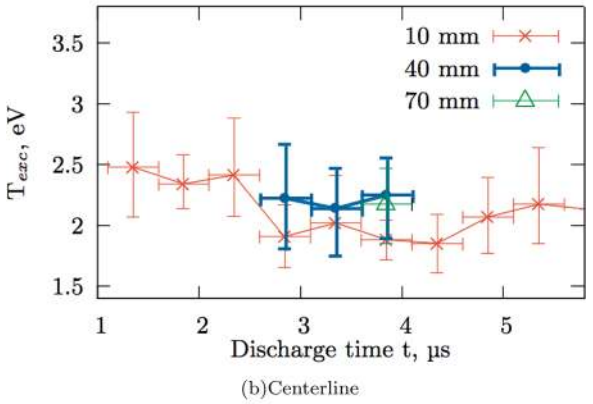

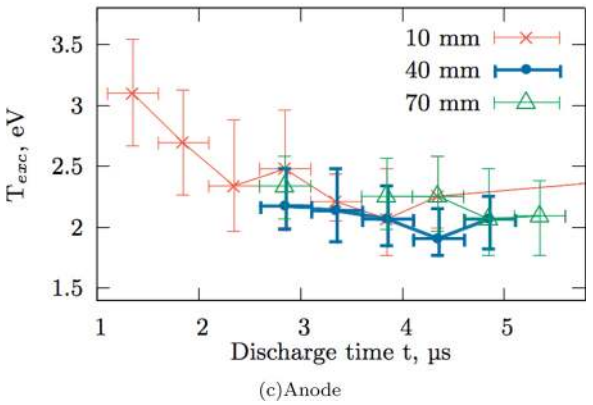

FIG. 8. Derived excitation temperature as a function of position and time for $C = 80\,\mu$F and $U = 1300$ V.

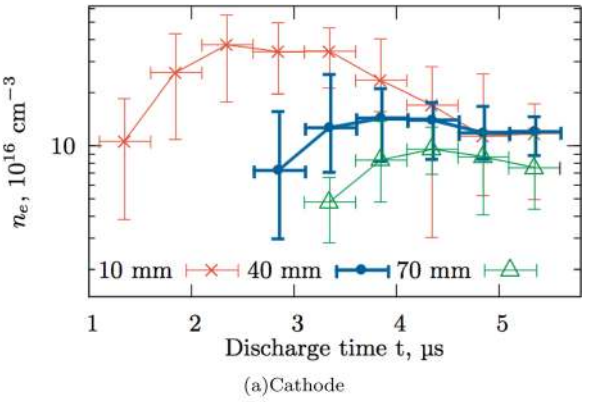

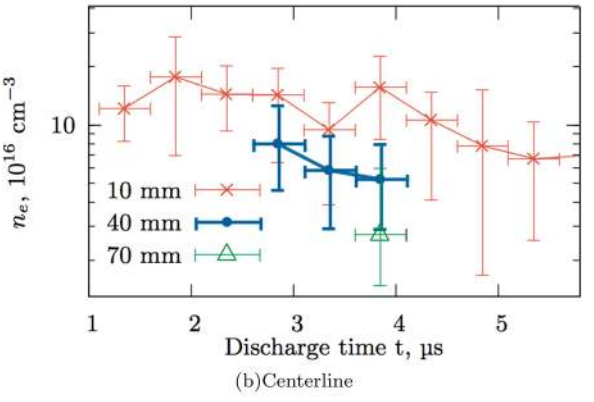

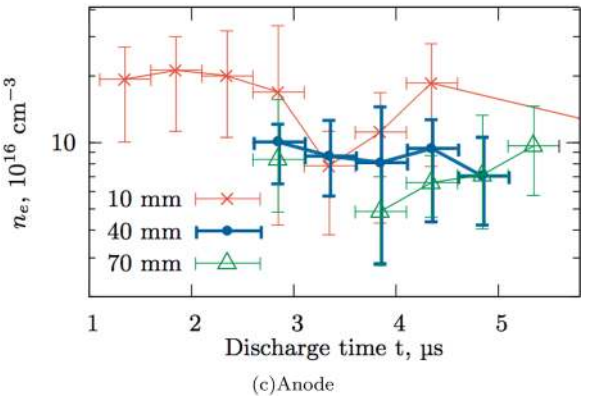

FIG. 9. Derived electron density as a function of position and time for $C = 80\,\mu$F and $U = 1300$ V.

in Fig. 9. Electron densities are in the order of 10^{17} cm^{-3} which is high compared to other electric propulsion systems, e.g., steady-state magnetoplasmadynamic (MPD) thruster (10^{13} cm^{-3}), Hall thruster (10^{12} cm^{-3}), or ion thruster (5×10^{11}cm^{-3}). Nevertheless, the values agree well with other researchers as well as with the previously shown findings although being slightly higher in average as shown in Table I.

As the plasma moves downstream, the values of electron density decrease, most likely due to the expansion of the plasma plume in combination with the time-dependent ionization-recombination processes. This effect can be seen at all positions of the cross section. The density is, in general, higher closer to the electrodes again favoring the conclusion of a higher energy density. However, the distribution stays constant for the entire acceleration channel as opposed to the homogeneous excitation temperature. Hence, the diffusion process in the cross section of the plasma bulk is most likely slower than the time of plasma motion. However, the significant uncertainty of the results defies more precise conclusions.

The influence of voltage and capacitance on the peak plasma parameters was investigated as well, and the results of peak temperature and electron density for the variation in voltage are plotted in Fig. 10. It is obvious that the decrease

TABLE I. Comparison of electron density.

Research	E_0 (J)	n_e range (10^{16} cm^{-3})
This work	68	2.7–37.3
Liu *et al.*[22]	5	2.534
Kazeev *et al.*[34]	100	0.4–1.3

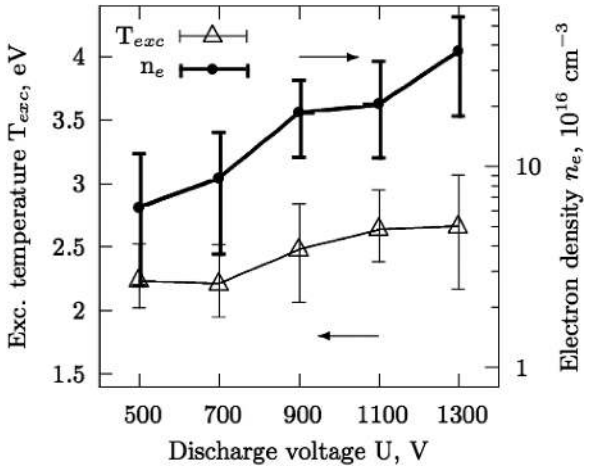

FIG. 10. Dependency of peak plasma parameters on discharge voltage.

in energy by the lower discharge voltage yields a plasma with lower temperature and density, respectively. For a reduction in capacitance, a peak excitation temperature at 1300 V on the centerline was found to be around 2.24 eV comparable to the values of high capacitance. The electron density, however, decreased from about 1.8×10^{17} cm^{-3} to about 9×10^{16} cm^{-3} on the centerline.

B. Mach-Zehnder interferometry

Measurements by means of Mach-Zehnder interferometry were conducted for a variation in time, discharge voltage, and capacitance. Four images were recorded for each permutation to cover the entire plasma area, and images for both wavelengths of the probe light taken. However, a first analysis showed that a fringe shift with reliable accuracy could only be detected in the area close to the propellant exit plane. Further, discharge voltages below 700 V for 80 μF-case and below 1100 V for 20 μF-case, respectively, yielded no variation in the fringe pattern. Figure 11 shows an example of the recorded interference pattern for a case without plasma (Fig. 11(a)) as well as with plasma (Fig. 11(b)).

In order to derive plasma properties from the images, the fringe shift number f (the ratio between interference fringe shift and fringe width) was derived from the images for 2 distinct lines of evaluation. The first line (line #1) was set parallel and close to the cathode, and the other line (line #2) was set parallel to the flow in the center of the plasma section shown in Fig. 11 which is about 7.5 mm from the centerline of the thruster. By using the fringe shift numbers derived from both probe light wavelengths, the electron density is derived by

$$n_e = \frac{8\pi^2 c^2 m_e \varepsilon_0}{e^2} \frac{f_1\lambda_1 - f_2\lambda_2}{d_p(\lambda_1^2 - \lambda_2^2)}. \quad (3)$$

The thickness of the plasma bulk d_p was derived to be 34.5 mm from photographic measurements. That is, only average values along the optical path can be obtained from Eq. (3). With the given resolution of the camera image and the signal-to-noise ratio, a minimum detectable electron density of 10^{16} cm^{-3} was derived for the setup. The dependency of the electron density on time and space is shown in Fig. 12. As the plasma moves further downstream, the density decreases rapidly, which confirms the tendency observed in the measurements by emission spectroscopy. Although the expected reliability of the values is higher for MZI than for emission spectroscopy, the detectable threshold defies the comparison of the values for positions further downstream. For $x = 10$ mm, the tendency on line #1 (Fig. 12(a)) agrees well with the values found at the measurement point close to the cathode (Fig. 9(a)). Therefore, one can assume that the order of magnitude and the general dependencies related to

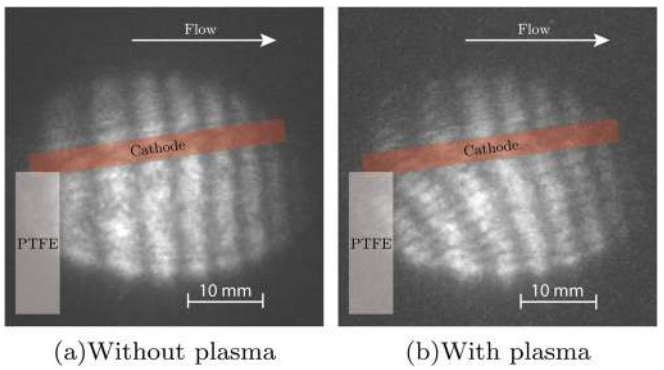

(a)Without plasma (b)With plasma

FIG. 11. Exemplary interference patterns recorded at $C = 80\,\mu$F and $U = 1300$ V.

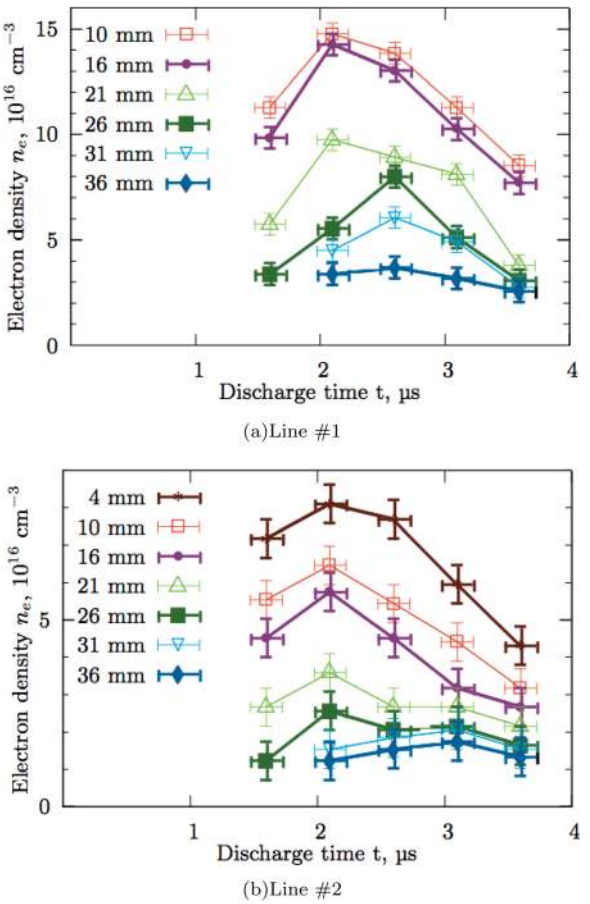

(a)Line #1

(b)Line #2

FIG. 12. Derived electron density by MZI for the 2 lines investigated as a function of time and space (x-direction). Results shown are for $C = 80\,\mu$F and $U = 1300$ V.

the electron density are verified by the MZI measurements. It is further obvious that the electron density decreases towards the centerline, as can be concluded by comparing the values of Figs. 12(a) and 12(b). However, the values for line #2 are smaller than the ones derived for the centerline (Fig. 9(b)) which might be a result of the different lines of sight for the two optical methods.

To determine the dependency on the discharge voltage, the peak electron density was determined over time for each energy setting. The resulting peak electron densities are plotted in Fig. 13 for the case of high capacitance. For a change between 700 up to 1100 V, the peak electron density increases accordingly, however, for the final voltage step up to 1300 V, only a small increase of only 10% in average is recognized. Reduction of the capacitance leads to a significant decrease in electron density similar to the results by emission spectroscopy. For the highest voltage, a peak electron density of about 3×10^{-16} cm^{-3} was determined, thus, a reduction of almost 80%.

One advantage of two-wavelength Mach-Zehnder interferometry is the further possibility to derive the neutral particle density under the assumption of single-ionized plasma by

$$n_n = \frac{\Delta N_1 - (K_i + K_{e1})n_e}{K_n}. \tag{4}$$

However, the effect caused by the presence of neutral particles was too small to be detectable, but an upper limit for the density can be derived from the threshold sensitivity of this method. With a fringe shift number of $f = 0.1$, the maximum neutral number density would be 10^{17} cm^{-3}. As the thruster accelerates the plasma by a magnetic field, one cannot assume the presence of neutral particles at all, but the results favor neither case. Spectral emission from neutral particles in Fig. 4 was in the same order as the noise.

In order to derive a minimum electron temperature, it is necessary to assume these neutral particles, LTE, and single-ionized plasma, so that the Eggert-Saha equation can be used by

$$\frac{n_i n_e}{n_n} = \frac{2Z_i}{Z_n}\left(\frac{2\pi m_e k T_e}{h^2}\right)^{3/2} e^{-\frac{U_i}{kT_e}}. \tag{5}$$

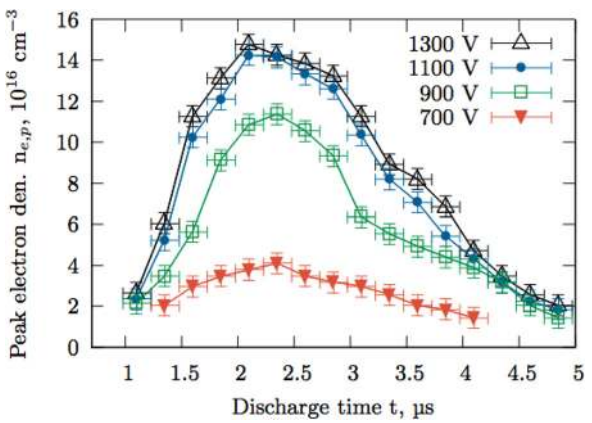

FIG. 13. Peak electron density as a function of time and discharge voltage for $C = 80\,\mu$F.

The values estimated by this equation with the upper limit of neutral density are about 2.1 eV for the peak electron density of 1.48×10^{17} cm^{-3} and 1.5 eV for the threshold electron density of 10^{16} cm^{-3}. These values are slightly lower than the ones derived by emission spectroscopy, but show the same order.

IV. DISCUSSION

With help of the experimentally measured plasma properties, it is possible to further classify the plasma. Using the electron temperature derived from emission spectroscopy together with the electron density measured by interferometry, the Debye length can be determined to be between 20 and 70 nm as a function of time and measurement position. With a characteristic length of 20 mm (initial distance between electrodes), the deviation of neutrality is less than $\mathcal{O}(10^{-6})$, and the plasma is therefore quasi neutral during the main acceleration phase. Further, the plasma can be considered ideal as the product $\frac{4\pi}{3} n_e \lambda_D^3$ is generally larger than 10. Landau lengths range between 0.5 and 1 nm. To determine the Knudsen number, Herdrich[35] showed that the mean free path can be calculated by

$$\lambda_{tot} = \frac{1}{\frac{1}{\lambda_{i-i}} + \frac{1}{\lambda_{i-e}}} = \frac{18\sqrt{2}\pi}{n_e \lambda_L^2 (36\pi^2 + \Lambda)}. \tag{6}$$

For the experimentally measured values within the plasma of ADD SIMP-LEX, the total mean free path lies between 50 and 200 μm. Hence, the Knudsen number is in the order of 0.001 to 0.01. These numbers indicate that the plasma might rather behave like a continuum flow than a particle flow. This conclusion is further supported by regarding the pressure in the plasma bulk. As the plasma is ideal, the ideal gas equation can validly be applied, leading to a pressure of about 0.3 atm. This value does not take into account the magnetic pressure that reaches a peak value of 4 atm with magnetic flux densities locally as strong as 1 T.[16] These high pressures would also favor a consideration of the PPT plasma as a continuum.

V. CONCLUSIONS

By means of emission spectroscopy and Mach-Zehnder interferometry, the plasma composition, the electron density, and electron temperature in the discharge plasma of a pulsed plasma thruster were determined as a function of measurement position, timing during the discharge, discharge voltage, as well as used capacitance. Values for the electron density lie in the order of 10^{17} cm^{-3} determined by Stark broadening from the spectral emission lines, and between 10^{16} and 10^{17} cm^{-3} determined from the interference fringes. In general, a good agreement between the two methods is found especially with regard to the inhomogeneous distribution in the cross section. The higher density as well as electron temperature closer to the electrodes suggests that the discharge arc causes a transition from the solid to plasma state with a slightly different energy density in the electrode-near regions. This was further supported by looking at the plasma composition, showing higher energetic species on the

center axis. Naturally, more energy is used in ionization (higher excitation/ionization state) rather than ablation (higher number density).

The values of electron density and electron temperature were further used to determine the Knudsen numbers in the flow field for the main plasma bulk indicating a continuum flow. Therefore, in order to model the behavior of the PPT discharge, the discrepancy between continuum models and particle models might be considerably small. This would confirm the past success of the slug model[5] to predict experimental values as it assumes the plasma to be accumulated in a single slug-like bulk. However, comparison with a particle code might still be required to verify this conclusion.

ACKNOWLEDGMENTS

T. Schönherr wants to acknowledge the support of the *Monbukagakusho* scholarship. F. Nees wants to thank the *Landesstiftung Baden-Württemberg* for their support during the research exchange. Further gratitude belongs to K. Shimamura for the experimental help as well as to C. Eichhorn for the discussion of the spectroscopic results.

[1]R. L. Sackheim, J. Propul. Power **22**, 1310 (2006).
[2]P. Molina-Cabrera, G. Herdrich, M. Lau, S. Fasoulas, T. Schönherr, and K. Komurasaki, "Pulsed plasma thrusters: a worldwide review and long yearned classification," in *32nd International Electric Propulsion Conference*, IEPC-2011-340, 2011.
[3]R. L. Burton and P. J. Turchi, J. Propul. Power **14**, 716 (1998).
[4]A. Rezaeiha and T. Schönherr, Aircr. Eng. **84**, 231 (2012).
[5]R. G. Jahn, *Physics of Electric Propulsion* (Dover, Mineola, NY, USA, 2006).
[6]T. Schönherr, K. Komurasaki, R. Kawashima, Y. Arakawa, and G. Herdrich, J. IAPS **18**, 23 (2010).
[7]T. Schönherr, K. Komurasaki, and G. Herdrich, World Acad. Sci. Eng. Technol. **50**, 557–563 (2011).
[8]A. Nawaz, R. Albertoni, and M. Auweter-Kurtz, Acta Astronaut. **67**, 440 (2010).
[9]T. Schönherr, K. Komurasaki, and G. Herdrich, "Propellant utilization efficiency in a pulsed plasma thruster," J. Propul. Power (submitted).
[10]T. E. Markusic, E. Y. Choueiri, and J. W. Berkery, Phys. Plasmas **11**, 4847 (2004).
[11]N. Kumagai, M. Igarashi, K. Sato, K. Tamura, K. Kawahara, and H. Takegahara, "Plume diagnostics in pulsed plasma thruster," in *38th AIAA/ASME/SAE/ASEE Joint Propulsion Conference*, AIAA Paper 2002-4124, 2002.
[12]H. Koizumi, R. Noji, K. Komurasaki, and Y. Arakawa, Phys. Plasmas **14**, 033506 (2007).
[13]A. Nawaz, U. Bauder, H. Böhrk, G. Herdrich, and M. Auweter-Kurtz, "Electrostatic probe and camera measurements for modeling the iMPD SIMP-LEX," in *43rd AIAA/ASME/SAE/ASEE Joint Propulsion Conference*, AIAA Paper 2007-5280, 2007.
[14]I. G. Krivonosov, M. M. Orlov, G. A. Popov, and V. N. Yakovlev, "The influence of energy storage capacitance on PPT characteristics," in *1st Annual International Conference on Small Satellites: New Technologies, Achievements, Problems and Prospects for International Co-Operation in the New Millennium*, Contribution III.11, 1998.
[15]G. G. Spanjers and R. A. Spores, "PPT research at AFRL: Material probes to measure the magnetic field distribution in a pulsed plasma thruster," in *34th AIAA/ASME/SAE/ASEE Joint Propulsion Conference*, AIAA Paper No. 98-3659, 1998.
[16]M. Lau, S. Manna, G. Herdrich, T. Schönherr, and K. Komurasaki, "Experimental investigation of the current density in the discharge plasma of ADD SIMP-LEX," in *48th AIAA/ASME/SAE/ASEE Joint Propulsion Conference*, AIAA Paper 2012-4275, 2012.
[17]M. Keidar, I. D. Boyd, E. Antonsen, and G. G. Spanjers, J. Propul. Power **20**, 961 (2004).
[18]N. A. Gatsonis, D. Juric, and D. P. Stechmann, "Numerical analysis of Teflon ablation in pulsed plasma thrusters," in *43rd AIAA/ASME/SAE/ASEE Joint Propulsion Conference*, AIAA Paper 2007-5227, 2007.
[19]E. M. Henrikson and P. G. Mikellides, "Modeling of ablation-fed pulsed plasma thruster operation using a new approach to the ablation process," in *44th AIAA/ASME/SAE/ASEE Joint Propulsion Conference*, AIAA Paper 2008-4645, 2008.
[20]M. N. Kazeev and V. F. Kozlov, "Ablation-fed discharge characteristics," in *31st International Electric Propulsion Conference*, IEPC-2009-249, 2009.
[21]T. E. Markusic and R. A. Spores, "Spectroscopic emission measurements of a pulsed plasma thruster plume," in *33rd AIAA/ASME/SAE/ASEE Joint Propulsion Conference*, AIAA Paper No. 97-2924, 1997.
[22]F. Liu, Z. Nie, X. Xu, Q. Zhou, L. Li, and R. Liang, Appl. Phys. Lett. **93**, 111502 (2008).
[23]Z. Mao, X. Zou, X. Wang, and W. Jiang, Appl. Phys. Lett. **94**, 181501 (2009).
[24]H. Zhang, J. Lu, Z. Shen, and X. Ni, Opt. Commun. **282**, 1720 (2009).
[25]K. Shimamura, K. Hatai, K. Kawamura, A. Fukui, A. Fukuda, B. Wang, T. Yamaguchi, K. Komurasaki, and Y. Arakawa, J. Appl. Phys. **109**, 084910 (2011).
[26]K. I. Thomassen and D. Tong, "Interferometric density measurements in the arc of a pulsed plasma thruster," in *9th Electric Propulsion Conference*, AIAA Paper No. 72-463, 1972.
[27]M. Fertig, D. Petkow, T. Stindl, M. Auweter-Kurtz, M. Quandt, C.-D. Munz, J. Neudorfer, S. Roller, D. D'Andrea, and R. Schneider, *in High Performance Computing in Science and Engineering'08* (Springer, Berlin, Germany, 2009), pp. 585–597.
[28]J. Neudorfer, T. Stindl, R. Schneider, S. Roller, C.-D. Munz, and M. Auweter-Kurtz, "Three-dimensional particle-in-cell simulation of a pulsed plasma thruster: Modeling and challenges," in *32nd International Electric Propulsion Conference*, IEPC-2011-116, 2011.
[29]D. Petkow, G. Herdrich, S. Fasoulas, and M. Auweter-Kurtz, "On the kinetic modeling of collisional effects relevant for non-stationary magnetoplasmadynamic thrusters," in *32nd International Electric Propulsion Conference*, IEPC-2011-307, 2011.
[30]E. J. Beiting, J. Qian, R. W. Russell, J. E. Pollard, W. Caven, and R. Corey, "Absolute emission form the mid-infrared to the extreme ultraviolet from a pulsed plasma thruster (PPT)," in *30th International Electric Propulsion Conference*, IEPC-2007-268, 2007.
[31]R. Eckman, L. Byrne, N. A. Gatsonis, and E. J. Pencil, J. Propul. Power **17**, 762 (2001).
[32]H. R. Griem, *Spectral Line Broadening by Plasmas*, Pure and Applied Physics, Vol. 39 (Academic, New York, NY, USA, 1974).
[33]H. R. Griem, *Plasma Spectroscopy* (McGraw-Hill Book, 1964).
[34]M. N. Kazeev, G. A. Popov, N. N. Antropov, G. A. Diakonov, M. M. Orlov, V. S. Posokhin, V. K. Tyutin, and V. N. Yakovlev, "Dynamics and distribution of electron density in the channel of pulsed plasma thruster," in *38th AIAA/ASME/SAE/ASEE Joint Propulsion Conference*, AIAA Paper 2002-4119, 2002.
[35]G. Herdrich, *Habilitation: Raumfahrtrelevante Plasmen und deren anwendungsbezogene Klassifizierung* (Universität Stuttgart, Stuttgart, Germany, 2012) (in German).